Numerical modeling of electrical-mechanical-acoustical behavior of a lumped acoustic source driven by a piezoelectric stack actuator

F. Tajdari [1], **A. P. Berkhoff** [2], **A. de Boer** [1]
[1] University of Twente, Department of Applied Mechanics,
Drienerlolaan 5, 7500 AE Enschede, The Netherlands
e-mail: **f.tajdari@utwente.nl**

[2] TNO, Technical Sciences, Acoustics and Sonar,
Oude Waalsdorperweg 63, 2597AK Den Haag, The Netherlands

Abstract
The present work describes the electrical, mechanical and acoustical behavior of a thin honey-comb structure as an acoustic source. The acoustic source has to operate in the low frequency, quasi-static regime and is driven by a piezoelectric stack actuator. In addition, a two-way energy flow between the actuator and a connected amplifier is investigated. In particular, the effectiveness of energy recovery from the reactive components of the acoustic source is evaluated to improve the overall radiation efficiency. A lumped model is used to represent the acoustic source that is excited by a stacked piezoelectric element. The required power supply and resulting radiation efficiency are evaluated when a conventional analogue amplifier is used. The result is compared to the case in which some parts of the stored power are recovered and sent back to the connected switching amplifier. The study reveals 20% increase in the radiation efficiency and more than 80% decrease in the amount of required input power through recovering the reactive power in the system.

1 Introduction

Designing acoustic sources, especially at low frequencies, has been recently investigated in specific applications; in active sound absorption or active noise control sources with severe space constraints, for example, for use in ducts. A flat acoustic source driven by voice coil actuators is introduced by reference [1] and is implemented to achieve a uniform, rigid body displacement [2]. This loudspeaker is supposed to generate a flat frequency response at low frequencies. Piezoelectric patch actuators have also been evaluated as the driving parts of this loudspeaker [3]. The electromagnetic actuators, which are used in the structure of this acoustic source, cause a large level of power dissipation.

Piezoelectric stack actuators are often used in smart structures due to their compact size and high efficiency. Potentially, they consume less electrical energy and have less energy loss than electromagnetic actuators. Various researches have been conducted to characterize piezoelectric elements. In [4–11], parametric identification of piezoelectric components is investigated. According to these studies, the stiffness, capacitance and other properties of piezoelectric actuators strongly depend on the electromechanical operating conditions. Moreover, the nonlinearity effects and thermo-electro-mechanical behavior [12] of piezoelectric stack actuators have been studied as well, especially at highly dynamic operations.

Piezoelectric stack actuators can particularly be used as the excitation part of acoustic sources. Therefore, piezoelectric stack elements can provide a large driving force with small displacement. In the present work, the conventional voice coil actuators in the structure of the suggested thin honey-comb acoustic source [1]

are replaced with the stacked piezoelectric elements; thus, it is expected that the overall efficiency of the loudspeaker can be improved.

However, piezoelectric stack actuators used in the structure of loudspeakers make the simulation procedure more complex. On the one hand, piezoelectric actuators are assumed to be purely capacitive at low frequencies [13–16]. As a result, a major portion of supplied power is stored in the reactive components of the piezoelectric elements. On the other hand, inefficient amplifiers connected to the piezoelectric devices can restrict the system to undergo large level of power loss [17]. Therefore, various amplifiers have been designed to improve the efficiency of the piezoelectric actuators by recovering the reactive power [18, 19].

In the present work, the electrical-mechanical-acoustical behavior of a single piezoelectric stack actuator is analytically and numerically explored. Then, as a case study, the performance of this actuator as the excitation part of a thin honey-comb acoustic source is investigated by using a lumped model. The performance of this loudspeaker is evaluated when the actuator is connected to analogue and switching amplifiers. The radiation efficiency of the acoustic source and the required power supply for the two different amplifiers are compared. By applying class D amplifiers with power recovery, a major portion of the reactive power stored in the piezoelectric element can be recovered due to the two-way power flow between the actuator and the connected amplifier [17]. Moreover, it is expected that the reactive power stored in the various mechanical and acoustical components of the acoustic source can also be recovered by using the switching amplifiers. Consequently, an improvement in the overall efficiency of the loudspeaker is expected. In the rest of this paper it is assumed that only those class D amplifiers are used that are capable of recovering the power.

2 Piezoelectric stack actuators

A piezoelectric stack actuator consists of several layers that are electrically in parallel and mechanically in series. In order to use it in the structure of an acoustic source, its parameters have to be characterized. Therefore, in this section, a multi-layer piezoelectric actuator is modeled both analytically and numerically. The single piezoelectric stack actuator with a clamped support at one end and an external force at the other end is simulated. When the applied force is zero, the piezoelectric actuator behavior resembles free vibration. Moreover, by modeling a sweep in the external force, the electromechanical response of the actuator is simulated in a semi-bocked condition. Increasing the amplitude of the external force continues until the applied force equals the piezoelectric blocked force. This force is the maximum force that can be applied to a piezoelectric element; therefore, under this force the amount of displacement of the element is zero. Hence, the actuator experiences a fully-bocked situation and cannot move any more.

2.1 Analytical model

There exist some methods to analytically model the electromechanical performance of a piezoelectric stack actuator. The most common one is to directly model the piezoelectric element based on constitutive equations. Another approach is using the equivalent electrical circuits of these kind of actuators.

2.1.1 Constitutive equations

One possible form of the piezoelectric constitutive equations is expressed as follows [13]:

$$\begin{aligned} S_{ij} &= s^E_{ijkl} T_{kl} + d_{kij} E_k \\ D_i &= d_{ikl} T_{kl} + \epsilon^T_{ik} E_k \end{aligned} \tag{1}$$

where S_{ij}, T_{kl}, D_i and E_k denote the strain tensors, stress tensors, electric displacement field and electric field components in the piezoelectric device, respectively, with $i, j, k, l = 1, 2, 3$, which show the direction of applied tensors and fields. Moreover, d_{kij}, s^E_{ijkl} and ϵ^T_{ik} represent piezoelectric constant, elastic compliance

constant and dielectric permittivity, respectively. The superscripts E and T indicate that the respective constants are evaluated at a constant electric field and at constant stress, respectively. According to Eq.(1), not only does the strain field in the piezoelectric materials depend on the stress field, but it is also a function of electric field. Moreover, the electrical displacement field is related to both the stress tensor and the applied electrical field.

2.1.2 Equivalent electrical circuits

As an alternate method, it is common to use equivalent electrical circuits for modeling the piezoelectric actuators instead of directly solving the constitutive equations; thus this approach is beneficial for simulating all the electrical, mechanical and acoustical domains simultaneously.

There are two main equivalent electrical circuits representing the electrical-mechanical-acoustical behavior of the piezoelectric actuators: three-port Mason and KLM electrical circuits. These models are identical to a three-port transfer function [16] – two ports for the mechanical input and output terminals, and one port for the input electrical current and voltage – which is able to predict all resonance and anti-resonance frequencies of the piezoelectric materials; however, these circuits are only valid for one piezoelectric layer. If multi-layer piezoelectric actuators are needed, some modifications are required to convert both introduced three-port circuits into two-port transfer functions. Our analytical simulation is carried out based on two equivalent electrical circuits of the Mason model represented in Fig. 1, and the parameters of the circuits are defined in Table 1. The first model is the simplified version of the circuit suggested by [14, 15], and the second one, which also takes the acoustical load of the air into consideration, is based on the circuit introduced by [16]. The second model is termed "Mason complex". In fact, the equivalent electrical circuit of a piezoelectric material consists of both electrical and mechanical parts which are interchangeable provided that a suitable conversion ratio is applied. Furthermore, in order to obtain more realistic results, the electrical and mechanical losses of the piezoelectric material have to be added to the model eventually.

To complete the analytical investigation, in the next step, the velocity of the free end of the vibrating piezoelectric actuator calculated from the equivalent electrical circuits is used to compute the acoustical variables of the actuator. Therefore, the sound pressure level on the free end of the piezoelectric actuator is calculated by evaluating the radiation impedance coupled with the resulting velocity of the free surface of the piezoelectric device which is computed via the analytical model. By considering the origin in the center of the vibrating surface, one can compute the SPL on the $z = 0$ plane by applying the following two equations [20–22]:

$$Z_{rad} = \rho_0 c_0 A(R_{rad} + iX_{rad}) \tag{2}$$

$$\begin{aligned} R_{rad} &= 1 - \frac{2J_1(2ka)}{2ka} \\ X_{rad} &= \frac{2K_1(2ka)}{2ka} \end{aligned} \tag{3}$$

for estimating the radiation impedance that is valid for vibrating pistons, where a is the radius of the piston, k is the wave number, and J_1 and K_1 are Bessel and Struve functions of the first kind, respectively. In addition, ρ_0 and c_0 represent the density and speed of sound in the medium, respectively, and A is the facing surface of the piston which is in interaction with the medium.

2.2 Numerical model

In order to make a comparison, in a case study, a subsequent numerical Finite Element simulation is performed in a 2D-symmetry space with respect to z axis in COMSOL Multi-physics package to solve the coupled fluid-structure-interaction problem; thus, the piezoelectric multi-layer device is simulated, and its behavior under, free, bocked and semi-blocked boundary conditions is compared with that of analytical model. In Fig 2 a piezoelectric stake actuator with one end clamped that is subjected to external force is represented based on blocked and semi-blocked boundary conditions.

Symbol	Meaning	SI Unit	Formula
V_{AC}	Total AC applied voltage	V	75
V_{DC}	Total DC applied voltage	V	75
V_{piezo}	Input voltage to the piezoelectric actuator	V	–
i_{piezo}	Input current to the piezoelectric actuator	A	–
i_t	Total supplied current to the amplifeir	A	–
i	Input current of the first transformer in the electrical domain	A	–
u	Velocity	$\mathrm{m\,s^{-1}}$	–
e	Input voltage of the 1^{st} transformer in the electrical domain	V	–
F_{in}	Output force of the 1^{st} transformer in the mechanical domain	N	–
F_{out}	Input force of the 2^{nd} transformer in the mechanical domain	N	–
P_{in}	Output pressure of the 2^{nd} transformer in the acoustical domain	Pa	–
U_d	Volume velocity	$\mathrm{m^3\,s^{-1}}$	–
U_1	Volume velocity trough the air cavity	$\mathrm{m^3\,s^{-1}}$	–
U_2	Volume velocity trough the hollows and the perforated plate	$\mathrm{m^3\,s^{-1}}$	–
A	Surface area	$\mathrm{m^2}$	–
R_E	External resistance	Ω	1
C_0	Piezoelectric blocked capacity	F	$\frac{\epsilon^T(1-{K_{33}}^2)A}{t}$
t	Piezoelectric thickness	m	$\frac{N}{l}$
k_{33}	Piezoelectric coupling factor	–	$\sqrt{\frac{d_{33}^2}{s^E\epsilon^T}}$
ϵ^T	Dielectric permittivity	–	–
N	Number of stack layers	–	–
l	Piezoelectric length	m	–
s^E	Elastic compliance	$\mathrm{m^2\,N^{-1}}$	–
d_{33}	Piezoelectric constant	$\mathrm{C\,N^{-1}}$	–
α	Conversion ratio	$\mathrm{C\,m^{-1}}$	$Nd_{33}K_p$
K_p	Piezoelectric stiffness	$\mathrm{N\,m^{-1}}$	$\frac{A}{ls^E}$
C_p	Piezoelectric compliance	$\mathrm{m\,N^{-1}}$	$\frac{1}{K_p}$
M_p	Piezoelectric effective mass	kg	$\frac{1}{3}m_{piezoelectric}$
Z_S	Mason complex capacitance	$\mathrm{kg\,s^{-1}}$	$\frac{\sin kl}{\Im(Z_{rad})\omega}$
Z_T	Mason complex inductance	$\mathrm{kg\,s^{-1}}$	$\frac{\Im(Z_{rad})\tan\frac{kl}{2}}{\omega}$
k	Wave number	$\mathrm{m^{-1}}$	$\frac{\omega}{c}$
Z_{mp}	Piezoelectric mass impedance	$\mathrm{kg\,s^{-1}}$	$\omega m_{piezoelectric}$
M_S	Total mass of the structure	kg	–
C_S	Total compliance of the structure	$\mathrm{m\,N^{-1}}$	–
R_S	Total damping of the structure	$\mathrm{N\,s\,m^{-1}}$	–
Z_{cavity}	Cavity acoustical impedance	$\mathrm{kg\,m^{-4}\,s^{-3}}$	$\frac{V_{cavity}}{\rho_{air}c^2}$
ρ_{air}	Air density	$\mathrm{kg\,m^{-3}}$	1.21
V	Volume	$\mathrm{m^3}$	–
c	Speed of sound in air	$\mathrm{m\,s^{-1}}$	343
Z_{screen}	Perforated plate acoustical impedance	$\mathrm{kg\,m^{-4}\,s^{-3}}$	$\frac{\rho_{air}c\zeta_{screen}}{A}$
Z_{rad}	Radiation impedance	$\mathrm{kg\,m^{-4}\,s^{-3}}$	Eq. (2)

Table 1: Parameters of the equivalent electrical circuit

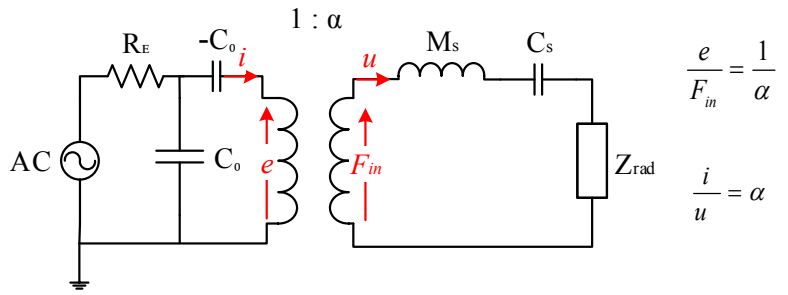

(a) Mason simplified model.

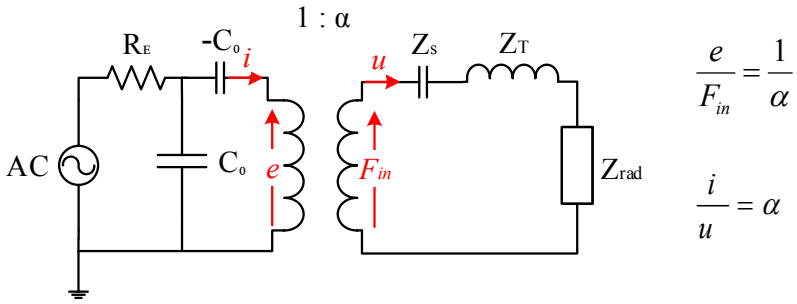

(b) Mason complex model.

Figure 1: Equivalent electrical circuits of a stack piezoelectric actuator in free vibration regime with one end clamped.

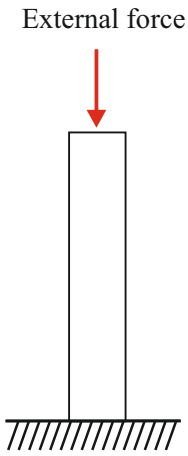

Figure 2: Blocked and semi-blocked boundary conditions.

2.3 Comparison between analytical and numerical approaches

The results in Fig. 3 and 4 show the free vibration behavior of the piezoelectric device under fixed voltage with the amplitude of 75 V AC that is biased by the DC voltage of 75 V. According to the graph in Fig. 3(a),

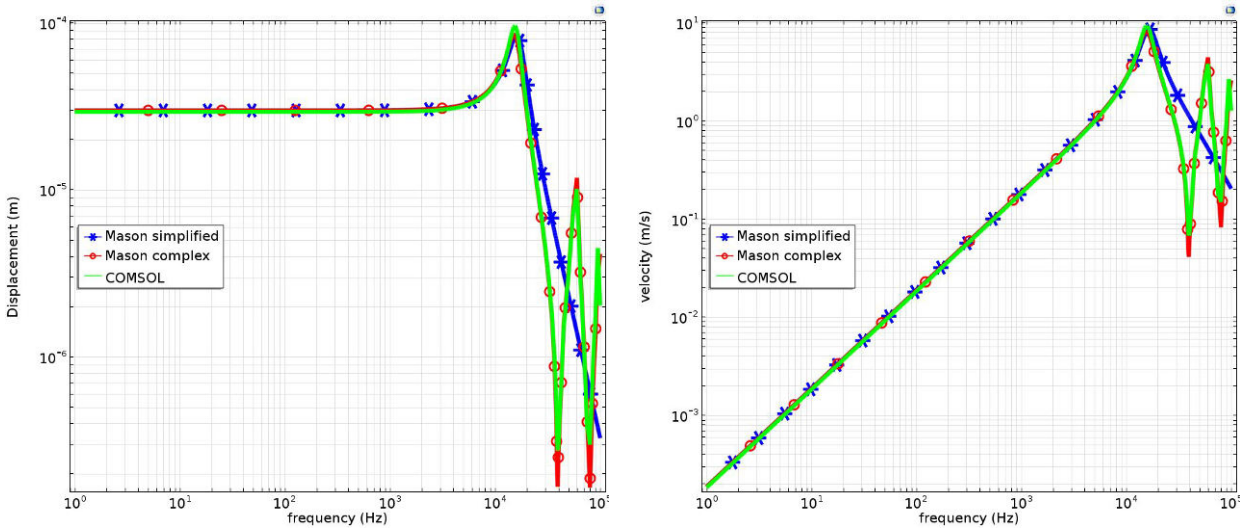

(a) Displacement. (b) Velocity.

Figure 3: Mechanical behavior of a single piezoelectric actuator in the free vibration regime with one end clamped

the free stroke of the piezoelectric actuator remains relatively constant below the resonance frequency and is predicted to be approximately 16 μm by both models. According to this graph, the displacement behavior of the piezoelectric device in the free vibration regime at the resonance frequency and at frequencies below the resonance frequency are in very close agreement. However, above the resonance, the FE model and the complex form of the Mason circuit can predict similar values of higher eigenfrequencies while the first analytical model, which is a simplified version of Mason electrical circuit, shows a different behavior in such prediction. This difference is due to assumption of neglecting the behavior of the piezoelectric element above the first resonance frequency. According to this assumption, the first model is only valid for frequencies below the resonance and cannot predict resonances and anti-resonances beyond this range. The velocity of the top surface of the piezoelectric in the free vibration regime is illustrated in Fig. 3(b). As it can be seen from the figure, as a result of both analytical and numerical simulations, the velocity experiences a gradual increase up to the resonance frequency. Figure 3 represents good agreement between the results of COMSOL simulation and those obtained from applying the analytical method.

Moreover, the characteristic diagrams of the piezoelectric actuator, such as displacement versus operating voltage, and displacement versus electrical impedance, are determined and compared with those obtained by the analytical solution in the free vibration regime in order to observe the electromechanical behavior of the actuator in frequencies below the resonance. For instance, Fig. 4 represents the Bode diagram of the electrical impedance of the piezoelectric material. As shown in Fig. 4(a), both numerical and analytical simulations predict a similar trend for the amplitude of the electrical impedance of the actuator below the resonance frequency. Likewise, both simulations predict a similar behavior for the changes in the phase of the electrical impedance starting from -90 degree as shown in Fig. 4(b).

In addition, both the bocked and semi-bocked boundary conditions are simulated in COMSOL. Figure 5 shows the results of such simulations under fixed voltage, similar to the one applied in the free vibration case, and frequency of 1000 Hz. Furthermore, the figure represents the mechanical behavior of the piezoelectric material under various external forces. Both the numerical simulation and the analytical model predict the blocked force to be approximately 1148 N. Moreover, Fig. 5 shows the linear relationship between the external force and the displacement of the piezoelectric actuator. There is a small offset between the analytical and numerical results that is due to the estimation of the radiation impedance of the piezoelectric device according to Eq. (2) in both electrical circuits.

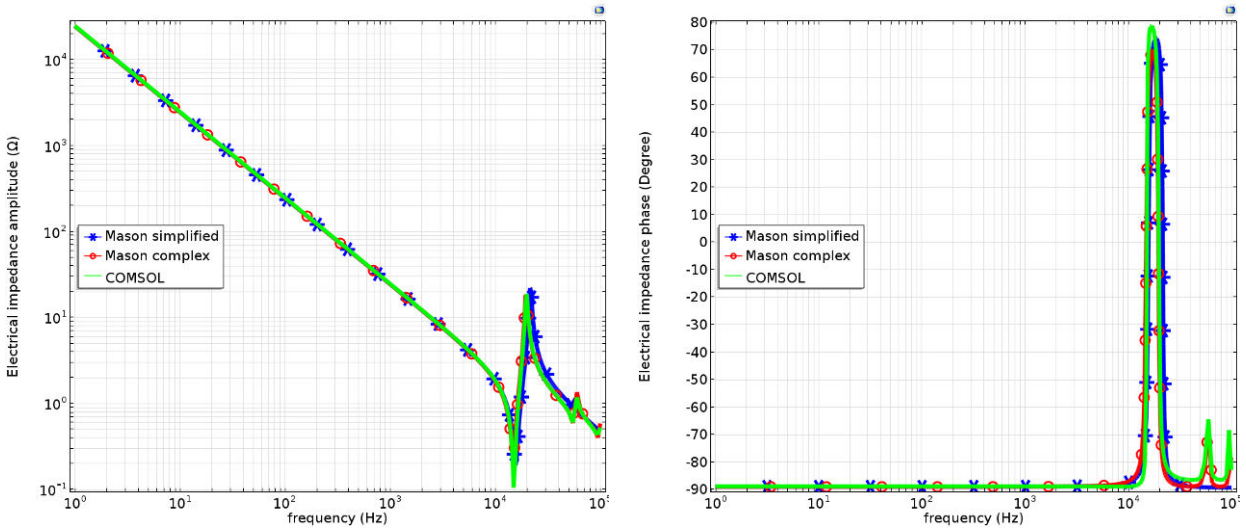

(a) Amplitude. (b) Phase.

Figure 4: Bode diagram of electrical impedance of a single piezoelectric actuator in the free vibration regime with one end clamped

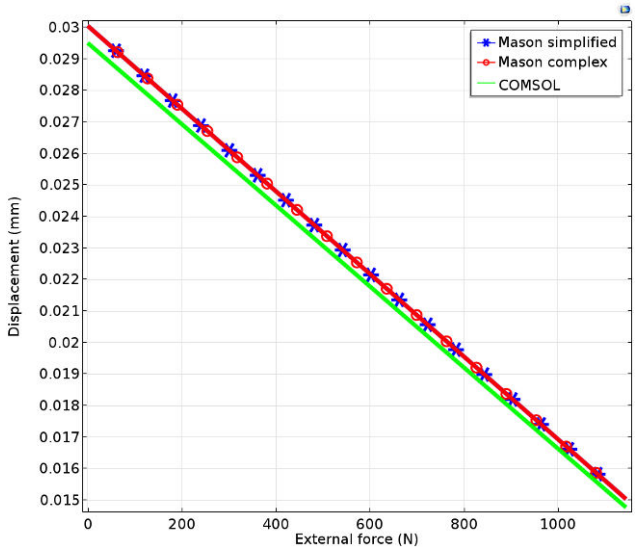

Figure 5: The characteristic diagram of a single piezoelectric stack actuator in semi-bocked regime with one end clamped under various external forces.

2.4 Experiment

In the next step, the suitable setup shown in Fig. 6(a) is used in order to perform experimental tests to verify the results of both the numerical simulation and the analytical method. During the experiments, the voltage and current of the piezoelectric actuator are measured at the fixed frequency of 1000 Hz. The free stroke of the actuator as a function of the applied voltage is shown in Fig. 6(b). From this figure, a comparison can be made between the models and the experiment. As it is clear from Fig. 6(b), the relationship between displacement and voltage is linear; however, there is an offset between the results of both models and that from the experiment. The offset is due to the fact that hysteresis loss is neglected during the modeling.

(a) Test setup for measuring the free stroke of the piezoelectric stake actuator with laser.

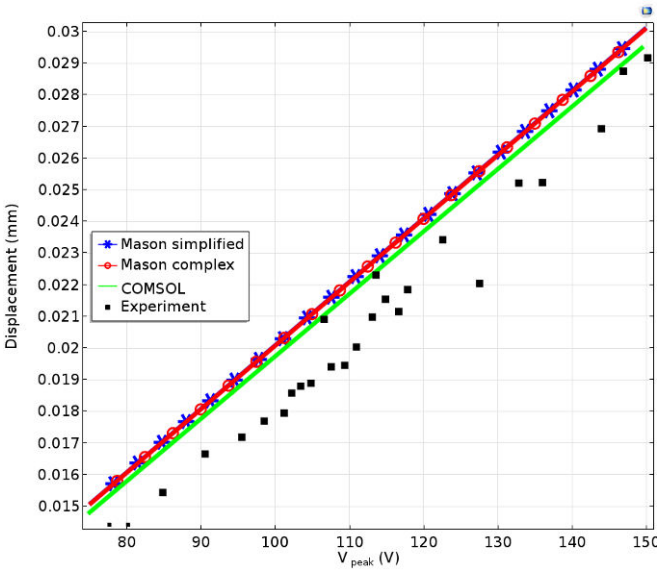

(b) Characteristics diagram of a single piezoelectric actuator in the free vibration regime with one end clamped under various applied voltage.

Figure 6: Experiment.

3 Amplifiers

To drive piezoelectric actuators, several amplifiers can be used. Due to the reactive nature of these actuators, a large level of power is stored in the reactive parts of the piezoelectric device when there is no power recovery [17–19]. Depending on the application, the required amplifier varies from the analogue type to the switching one. If the precision positioning is desired, analogue amplifiers can provide the best quality of the output signal. Indeed, they can continuously transfer the supplied power to the piezoelectric elements during charge and discharge cycles. However, a large portion of supplied power is dissipated in the analogue amplifier unit since during discharge, the transfered power to the piezoelectric actuator is not needed. As a result of the power loss, class A amplifiers have poor efficiency below 50%. Therefore, such amplifiers are mainly used in the applications in which the quality outweighs the poor efficiency.

On the other hand, switching amplifiers are appropriate for applications in which the efficiency is the target. In fact, they are capable of lowering the power loss in the output stage of amplifier unit and while minimizing the power required for the piezoelectric element. Moreover, they can recover the reactive power stored in the piezoelectric device during discharge. Consequently, they can achieve a typical efficiency of 95%.

The power flow for a single piezoelectric stack actuator is shown in Fig. 7. The amount of power required for the analogue (class A) and switching (class D) amplifiers, which are connected to the piezoelectric actuator, is represented in this figure. According to Fig. 7(a), class A amplifiers have to be supplied by double the power required for the piezoelectric element. Eventually, all the input power is dissipated due to the fact that no power recovery is possible in class A amplifiers. However, when a class D amplifier is used, only 40.8% of the power needed for the piezoelectric device is required for the amplifier (Fig. 7(b)). In fact, in this case, the major part of the reactive power, which is stored in the piezoelectric element, is recovered and can be reused in the next cycle. Therefore, using the switching amplifiers can save significant amount of power.

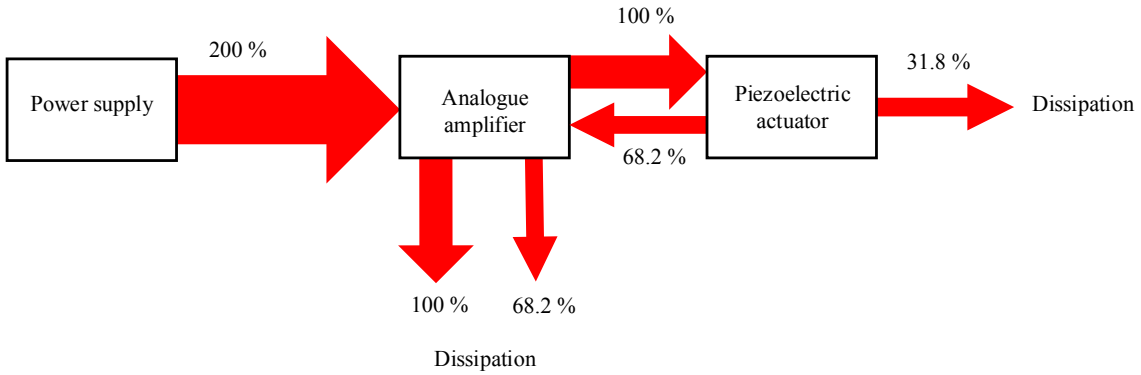

(a) Class A amplifier.

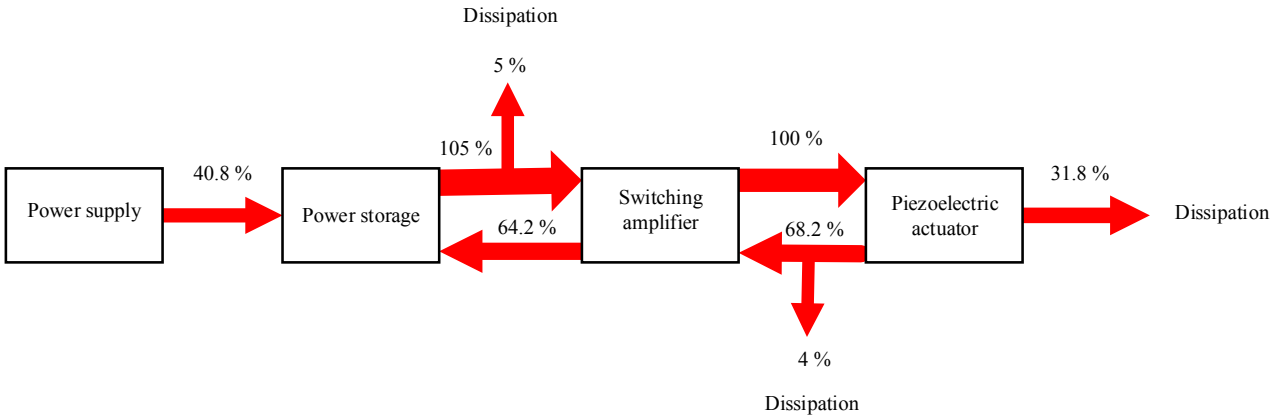

(b) Class D amplifier with power recovery.

Figure 7: Power flow through a single piezoelectric stack actuator connected to analogue and switching amplifiers.

4 Case study: thin honey-comb acoustic source

4.1 Honey-comb structure

The simulated stack piezoelectric actuator is used as the excitation part of the thin honey-comb structure [1]. As it is shown in Fig. 8, the acoustic source is a vibrating plate. it has a relatively large surface area (60.5 cm $\times$ 41.5 cm) and a relatively small thickness (22 mm). At low frequencies (16 Hz to 1000 Hz), a large volume displacement is required for the acoustic source in order to radiate a sufficient amount of acoustical power. If the source is thin, then a relatively large surface area is required. To prevent undesirable bending mode shapes, the plate is attached to the top surface of a honey-comb structure; thus, the rigid displacement of the structure is achieved when the first bending mode of the combined structure is not in the range of 16 Hz to 1000 Hz. A perforated plate is attached to the bottom surface of the honey-comb. This plate is in interaction with a cavity in the lower part of the loudspeaker; as a result, the air inside the cavity can enter and leave the honey-comb structure through the holes of the perforated plate during the operation of the loudspeaker. Actuators excite the acoustic source in the out-of-plane direction.

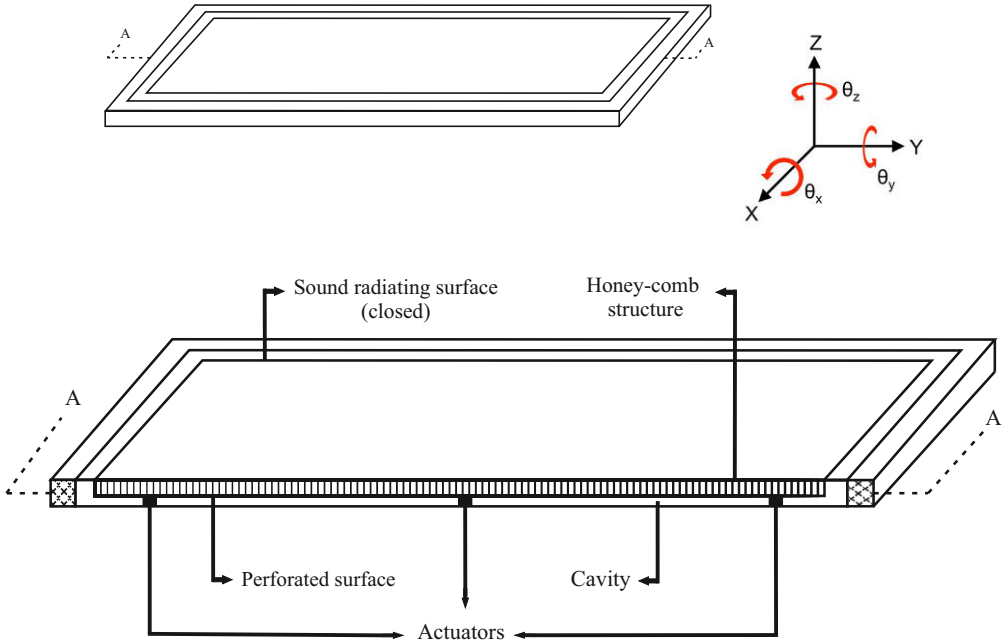

Figure 8: The acoustic source based on a honey-comb structure with A–A cross section view.

4.2 Lumped model

The lumped model of the whole loudspeaker, including the perforated honey-comb structure, cavity and single piezoelectric actuator, is analytically modeled. The equivalent electrical circuit of the acoustic source driven by one piezoelectric stack actuator is shown in Fig. 9, and the parameters of the circuit are defined in Table1. According to Fig. 9, all electrical, mechanical and acoustical domains are modeled as individual electrical circuits that are connected to each other by using transformers. In the electrical domain, the biased AC voltage of 75 V is applied to the amplifier, which is connected to the actuator. The dielectric loss of the piezoelectric actuator is also taken into account in this model. In the mechanical domain, the mechanical impedance of the piezoelectric device regarding the "Mason complex circuit" is considered. In addition, the mass of the honey-comb structure, and the damping and compliance of the external springs are accounted for. The acoustical domain contains the acoustic impedances of the cavity, perforated plate and hollows of the honey-comb structure. Moreover, the radiation impedance of the vibrating plate forms another part of the acoustical circuit. The real part of the radiation impedance shows the resistivity of the surrounding air. This real part is responsible for radiating sound in the air. On the other hand, the imaginary part of the radiation impedance is associated with the load imposed by the air on the top surface of the vibrating plate. The air load resembles the mass of the air layer on the top surface of the vibrating plate which resists against the vibration.

4.3 Power supply

To complete the simulation procedure, the effect of connected amplifier on the performance of the acoustic source is investigated. The power flow chart for the loudspeaker is shown in Fig. 10. There is an improvement in the performance of the acoustic source when the piezoelectric device is connected to a class D amplifier compared to the case it is connected to a class A amplifier. Total electrical power required as the input of the piezoelectric device is:

$$P_{piezoelectric} = 0.5(V_{piezo} \cdot i^*_{piezo}) \tag{4}$$

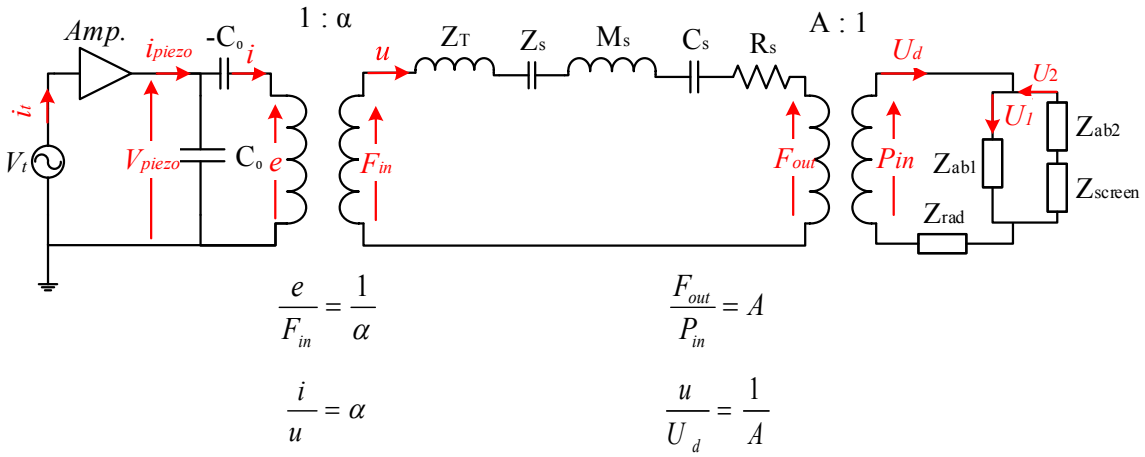

Figure 9: Lumped equivalent electrical circuit of the perforated honey-comb loudspeaker driven by one stack piezoelectric actuator.

where i^*_{piezo} and V_{piezo} are the complex conjugate of the current through the piezoelectric device and the voltage across the piezoelectric element, respectively. Equation (4) can also be formulated by its active and reactive components as follows

$$P_{piezoelectric} = P_{active,piezo} + jP_{reactive,piezo} \tag{5}$$

in which the active and reactive parts can be computed by using the following equations:

$$P_{active,piezo} = 0.5\Re(V_{piezo} \cdot i^*_{piezo}) \tag{6}$$

$$P_{reactive,piezo} = 0.5\Im(V_{piezo} \cdot i^*_{piezo}) \tag{7}$$

In case class D amplifiers are used, only 38.9% of the power calculated by Eq. (4) is required. In fact, if switching amplifiers are used, the total reactive power stored in the capacitance of the piezoelectric actuator, and a fraction of the reactive power stored in the mechanical and acoustical domains have the potential to be recovered. The amount of recovered power is evaluated using:

$$P_{recovery} = P_{C_E,piezo} + k_{33}(P_{C_M,piezo} + P_{cavity} + P_{rad,m}) \tag{8}$$

in which, k_{33} is the coupling factor of the piezoelectric device. Moreover, term $P_{C_E,piezo}$ denotes the reactive power stored in the capacitance of the piezoeletric actuator and can be calculated as follows:

$$P_{C_E,piezo} = 0.5\Im(V^2_{piezo} \cdot (C_0 j\omega)^*) \tag{9}$$

where ω is the angular frequency in $\mathrm{rad\,s^{-1}}$ and C_0 is defined in Table 1. The reactive power stored in the mechanical stiffness of the piezoelectric device, $P_{C_M,piezo}$, is computed using Table 1:

$$P_{C_M,piezo} = 0.5\Im(u^2 \cdot Z^*_S) \tag{10}$$

Reactive power stored in the cavity (P_{cavity}) and air load on the vibrating plate ($P_{rad,m}$) are formulated as follows:

$$P_{cavity} = 0.5\Im(U_1^2 \cdot Z^*_{cavity}) \tag{11}$$

$$P_{rad,m} = 0.5\Im(U_d^2 \cdot Z^*_{rad}) \tag{12}$$

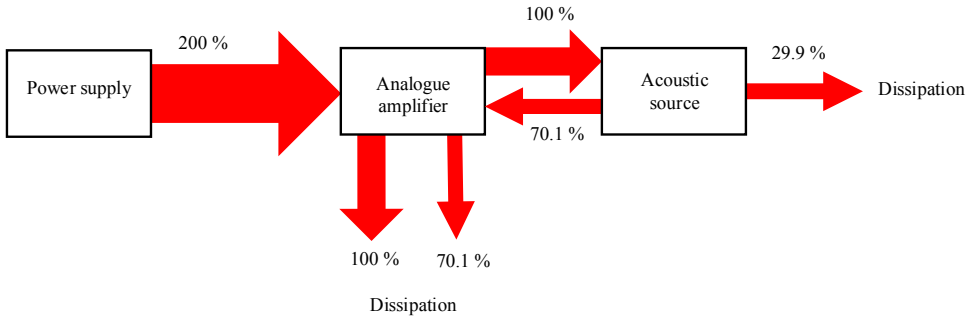

(a) Class A amplifier.

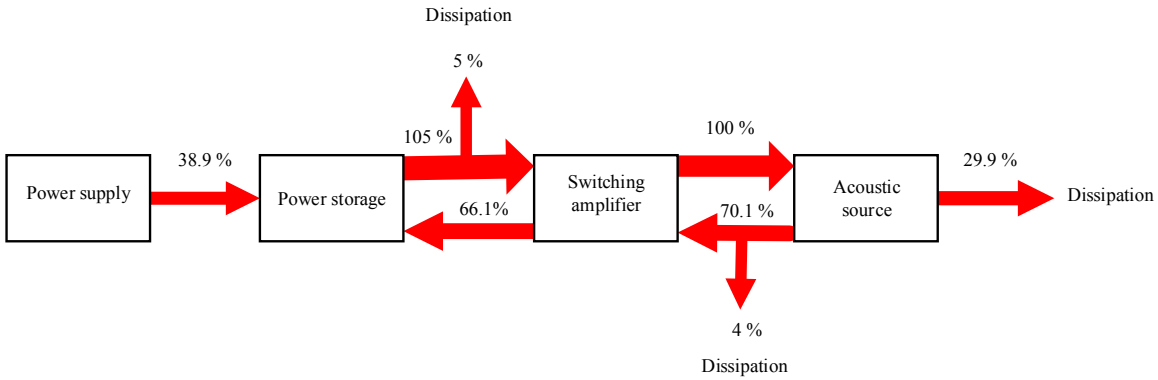

(b) Class D amplifier with power recovery.

Figure 10: Power flow through the lumped acoustic source.

let U_d denote volume velocity of the air, then U_1 is the volume velocity of the air in the cavity in $\mathrm{m}^3\,\mathrm{s}^{-1}$. According to Fig. 10 and Eq. (8), the power recovery forms approximately 70.1% of the piezoelectric element input power. Therefore, only 29.9% power dissipation occurs in the system.

Figure 11 represents the efficiency of the loudspeaker. The efficiency is computed by:

$$\eta_{rad} = \frac{P_{rad}}{P_{E,active}} \tag{13}$$

which is the ratio of the dissipated acoustical power through the sound radiation to the active part of the total input power and can be calculated using the following equations:

$$P_{rad} = 0.5\Re(U_d^2 \cdot Z_{rad}^*) \tag{14}$$

$$P_{E,active} = 0.5\Re(V_t \cdot i_t^*) \tag{15}$$

where the total applied electrical power can be represented by using the equations below:

$$P_{E,total} = 0.5(V_t \cdot i_t^*) \tag{16}$$

$$P_{E,total} = P_{E,active} + P_{E,reactive} \tag{17}$$

In Eqs. (15) to (17), V_t and i_t are the applied voltage to the amplifier and the resulting current, respectively. In case analogue amplifiers are used, all the supplied power is dissipated eventually in the system since no

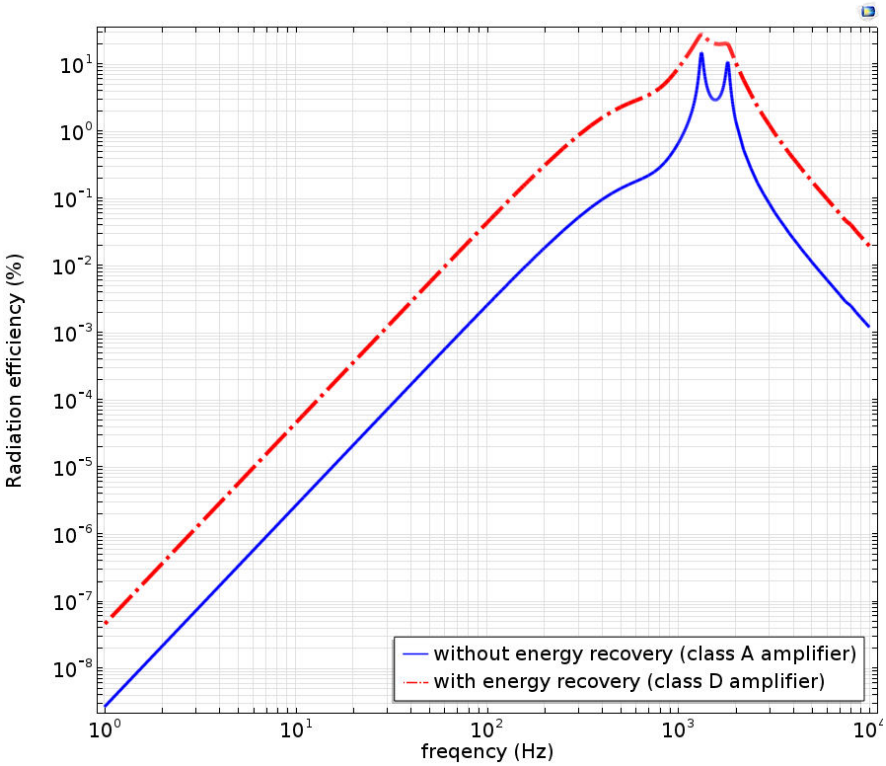

Figure 11: Efficiency of the acoustic source when it is connected to analogue and switching amplifiers.

power recovery is possible. However, according to Fig. 10, when a switching amplifier is used, up to 66.1% of the actual required power can be sent back to the amplifier and, consequently, the overall efficiency of the acoustic source is improved. For frequencies below 100 Hz, the efficiency slightly increases. In addition, at resonance frequency the efficiency can be improved more than 20%.

5 Conclusion

The characteristics of a multi-layer piezoelectric actuator in free, bocked, and semi-bocked boundary conditions are investigated. The study reveals that both Mason circuits are in agreement with the COMSOL simulation below the first resonance frequency. In addition, it is concluded that only the complex form of the Mason circuit fully agrees with the numerical model, and is capable of predicting the mechanical behavior of the piezoelectric actuator above the first eigenfrequency. The experiment validates both analytical and numerical models; however, there is an offset between both simulations and reality due to the existence of hysteresis. Then, the actuator, which is modeled by "Mason complex" circuit, is used as the excitation part of a thin honey-comb acoustic source. The performance of such an acoustic source is evaluated when analogue and switching amplifiers are connected to the piezoelectric device. For the particular configuration studied in this paper, class D amplifiers with power recovery can improve the radiation efficiency up to 35% while recovering approximately 66% of the reactive power stored in the acoustic source.

Acknowledgements

The authors gratefully acknowledge the European Commission for its support of the Marie Curie program through the ITN ANTARES project (GA 606817).

References

[1] A. P. Berkhoff, *Sound generator*, US Patent US20 100 111 351 A2 (2010).

[2] J. Ho, *Control source development for reduction of noise transmitted through a double panel structure*, Ph.D. thesis, University of Twente, Enschede, The Netherlands, 2014 July.

[3] J. H. Ho, A. Berkhoff, *Flat acoustic sources with frequency response correction based on feedback and feed-forward distributed control*, The Journal of the Acoustical Society of America, vol. 137, No. 4, pp. 2080-2088 (2015).

[4] M. Mitrovic, G. P. Carman, F. K. Straub, *Electro-mechanical characterization of piezoelectric stack actuators*, *Proceedings of SPIE Conference (1999)*, vol. 3668, No. 99, pp. 586-601.

[5] L. R. Corr, W. W. Clark, *Comparison of low frequency piezoceramic shunt techniques for structural damping*, *Proceedings of SPIE Conference (2001)*, vol. 4331, No.1, pp. 262-272.

[6] V. Giurgiutiu, R. Pomirleanu, *Comparison of low frequency piezoceramic shunt techniques for structural damping*, J. of Smart Mater. Struct. (2002), vol. 1627, No.2, pp. 370-376.

[7] R. Pomirleanu, V. Giurgiutiu, *Full-strock and dynamic analysis of high-power piezoelectric actuators*, Journal of Intelligent Material Systems and Structures (2002), vol. 13, pp. 275-289.

[8] Z. Kaiu, Y. Shaoze, W. Shizhu, *Influence of electro-mechanical loading on mechanical characterization of piezoelectric stack actuators*, *Proceedings of SPIE Conference (2003)*, vol. 5253, pp. 940-943.

[9] D. E. Heverly II, K. W. Wang, E. C. Smith, *Dual-stack piezoelectric device with bidirectional actuation and improved performance*, Journal of Intelligent Material Systems and Structures (2004), vol. 15, pp. 565-574.

[10] M. N. Ghasemi-Nejhad, S. Pourjalali, M. Uyema, A. Yousefpour, *Finite element method for active vibration suppression of smart composite structures using piezoelectric materials*, Journal of Thermoplastic Composite Materials (2006), vol. 19, pp. 309-351.

[11] S. Sherrit, C. M. Jones, J. B. Aldrich, C. Blodget, X. Bao, M. Badescu, Y. Bar-Cohen, *Multilayer piezoelectric stack actuator characterization*, *Proceedings of SPIE Conference (2008)*, vol. 6929, No. 9, pp. 1-12.

[12] F. X. Li, R. K. N. D. Rajapakse, D. Mumford, M. Gadala, *Quasi-static thermo-electro-mechanical behaviour of piezoelectric stack actuators*, J. of Smart Mater. Struct. (2008), vol. 17, pp. 1-10.

[13] American National Standards Institute and IEEE Ultrasonics, Ferroelectrics, and Frequency Control Society, Standards Committee and Institute of Electrical and Electronics Engineers, *IEEE Standard on Piezoelectricity*, ANSI/IEEE std 176-1987.

[14] L. L. Beranek, T. J. Mello, *Acoustics: Sound Fields and Transducers*, ELSEVIER Press (2012), pp. 98-101.

[15] M. Rossi, *Acoustics and electroacoustics*, Artech House (1988), pp. 353-373.

[16] A. Arnau, *Piezoelectric Transducers and Applications*, Springer (2004), pp. 60-63.

[17] H. Janocha, Ch. Stiebel, Th. Wurtz, *Power amplifiers for piezoelectric actuators*, A. Preumont (ed.), Responsive Systems for Active Vibration Control, Kluwer Academic Publishers (2002), pp. 379-391.

[18] H. Liang, Z. Jiao, R. Zhang, X. Wang, X. Liu, *Design of a power amplifier with energy recovery strategy for piezoelectric actuators*, IEEE, Vol. 2, No. 11, (2011), pp. 207-212.

[19] D. Vasic, F. Costa, *Energy recovery power supply for piezoelectric actuator*, IEEE, Vol. 5, No. 14, (2014), pp. 1440-1445.

[20] H. Levine, *On the radiation impedance of a rectangular piston*, The Journal of the Acoustical Society of America (1985), vol. 89, no. 4, pp. 447-455.

[21] F. Fahy, J. Walker, *Advanced applications in acoustics, noise and vibration*. Spon Press (2004), pp. 80-82.

[22] R. M. Aarts, A. J. E. M. Janssen, *Approximation of the Struve function H_1 occurring in impedance calculations*, The Journal of the Acoustical Society of America, vol. 113, No. 5, pp. 2635-2637 (2003).